Title: **The axonal localization of Dual Leucine Zipper Kinase defines its protein-turnover**

Seungmi Kim, Yaw Quagraine, Monika Singh, Jung Hwan Kim*

Department of Biology, University of Nevada, Reno, Reno, NV 89557

*Correspondence: jungkim@unr.edu

Summary

Subcellular protein localization plays critical roles in diverse neuronal functions. Dual Leucine Zipper Kinase (DLK) mediates neuronal stress responses including neuronal loss in multiple neurodegenerative disorders. DLK is axonally expressed, and its expression is constantly suppressed under normal conditions. However, little is known about how and why DLK is localized in axons. We found that Wallenda (Wnd), the *Drosophila* ortholog of DLK, is highly enriched in the axon terminals and this localization is necessary for the Highwire-mediated suppression of Wnd protein levels. We further found that a palmitoylation on Wnd plays an essential role in its axonal localization. Inhibiting axonal localization of Wnd resulted in dramatically increased protein levels of Wnd, which led to excessive stress signaling including neuronal loss. Our study demonstrates that subcellular protein localization is coupled with regulated protein turnover in neuronal stress response.

18 Keywords

19 DLK, axonal localization, regulated protein turnover, Highwire, protein palmitoylation, HIP14,

20 stress response, neurodegeneration

21

22 Highlights

23 - Wnd is highly enriched in the axon terminals.
24 - Wnd protein turnover by Hiw is restricted in axons.
25 - Wnd Palmitoylation is essential for its axonal localization, thus for its protein turnover.
26 - Palmitoylation-deficient Wnd exacerbates neuronal loss by deregulated protein
27 expression.

Introduction

A typical neuron is composed of somatodendritic and axonal compartments that are morphologically and functionally distinct, which is essential for a functioning nervous system. Distinct compositions of membrane and cytoplasmic proteins in each compartment represent its functions and are precisely established, maintained by an intricate network of intracellular transport (Guedes-Dias and Holzbaur, 2019; Guillaud et al., 2020). Consistently, defective neuronal intracellular transport was reported as an early cellular event in various neurodegenerative disorders including amyotrophic lateral sclerosis (Collard et al., 1995; De Vos and Hafezparast, 2017), Alzheimer's (Calkins et al., 2011; Wang et al., 2015), Parkinson's (Saha et al., 2004; Chu et al., 2012), and Huntington's diseases (Lee et al., 2004; Reddy and Shirendeb, 2012; Smith et al., 2014).

Dual Leucine Zipper Kinase (DLK), also known as MAP3K12 is a cytoplasmic protein kinase essential for stress signaling and mediates diverse neuronal responses including axon regeneration, axon degeneration, and cell death (Miller et al., 2009; Xiong et al., 2010; Shin et al., 2012; Xiong and Collins, 2012; Watkins et al., 2013; Li et al., 2021). To avoid excessive stress signaling, neurons tightly control DLK activity mainly through suppressing protein expression levels by an evolutionarily conserved PHR1/RPM-1/Highwire (Hiw) ubiquitin ligase (Nakata et al., 2005; Collins et al., 2006; Xiong et al., 2010; Huntwork-Rodriguez et al., 2013). Remarkable, recent studies have shown the likely widespread role of DLK in neuronal death from neurotrophic factor deprivation, glaucoma, amyotrophic lateral sclerosis, and Alzheimer's disease models (Pozniak et al., 2013; Welsbie et al., 2013, 2017; Larhammar et al., 2017a; Le Pichon et al., 2017; Patel et al., 2017a). These observations also imply the upregulated or deregulated DLK protein levels in these diseases. Interestingly, DLK proteins are present in the axonal compartments (Xiong et al., 2010; Klinedinst et al., 2013; Holland et al., 2016; Niu et al., 2020, 2022). Although a widely accepted model provides an elegant mechanism of axonal

53 retrograde signaling by axonally expressed DLK proteins (Yan et al., 2009; Xiong et al., 2010;
54 Shin et al., 2012; Larhammar et al., 2017b; Asghari Adib et al., 2018), little is known about how
55 and why DLK is expressed in axons and whether this localization plays a role in neuronal stress
56 response.

57 Here, we report a novel coupling between axonal localization and protein turnover of DLK. We
58 found that Wallenda (Wnd), *Drosophila* DLK is highly enriched in the axon terminals of
59 *Drosophila* sensory neurons and that Wnd protein turnover by Hiw is restricted to the axons.
60 Furthermore, we identified a crucial motif on Wnd - a protein palmitoylation - that is necessary
61 for axonal localization but does not affect DLK signaling capacity. Inhibiting axonal transport of
62 Wnd caused a massive accumulation of Wnd proteins in neuronal cell bodies, which resulted in
63 excessive stress signaling and subsequent neuronal loss. Together, our findings demonstrate
64 the importance of DLK protein transport in neuronal stress responses.

65 Result

66 **Wnd is highly enriched in the axon terminals.**

67 DLK genes encode cytosolic proteins but are found in the axonal compartments of diverse
68 animals (Holland et al., 2016; Niu et al., 2020, 2022). To understand the role of DLK axonal
69 localization, we first set out to test the extent of axonal localization of *Drosophila* DLK, Wallenda
70 (Wnd). We took advantage of a *wnd* protein-trap allele, *Mi{MIC}wnd*^{GFSTF}, which allows us to
71 visualize endogenous Wnd protein expression via an EGFP tag (Venken et al., 2011; Li et al.,
72 2017). The levels of Wnd-GFSTF proteins in the third instar larva stage were extremely low. To
73 enhance detection of Wnd-GFSTF, the experiment was performed in *highwire* (*hiw*) mutants,
74 *hiw*$^{\Delta N}$ (Wu et al., 2005). Hiw is a neuronal ubiquitin ligase that selectively targets Wnd for protein
75 degradation. The third instar larvae were immunostained with anti-GFP antibody and examined
76 under a confocal microscope. The result showed a strikingly polarized expression pattern of
77 Wnd. While Wnd-GFSTF expression was evident in the neuropil region in the ventral nerve cord
78 (VNC), we could not detect any meaningful signal from the neuronal cell bodies, especially from
79 the peripheral nervous system neurons (**Figure 1A**). Neuropils are enriched in neural dendrites
80 and axons while mostly devoid of neuronal cell bodies.

81 To dissect the mechanisms underlying Wnd protein localization, we turned to a transgene
82 approach. Selective protein expression can be achieved by various ways including local protein
83 synthesis, selective protein retention and degradation, and protein transport. Local protein
84 synthesis requires transport of mRNAs to a cellular compartment, which often requires
85 sequence motifs in the untranslated region (UTR) of an mRNA. We generated the Wnd-GFP
86 transgenes with and without *wnd*-UTR. The Wnd transgenes were specifically expressed in the
87 larval sensory neurons (C4da) using *ppk-GAL4* (Grueber et al., 2007). These neurons position
88 their cell body in the larval body wall where they elaborate dendrites while sending their axons
89 to the larval central nervous system — the VNC, hence provide an excellent tool to study

90 localized protein expression in the cell body, dendrites, and axons (Grueber et al., 2007). We
91 measured expression levels of Wnd transgenes in the cell body and in the axon terminals of
92 C4da neurons using confocal microscope imaging. Their expression levels were normalized by
93 a general membrane marker, mCD8::RFP. The result showed a striking enrichment of Wnd in
94 the axon terminals of C4da neurons regardless of the UTR (**Figure 1B** and **1D**), which suggests
95 that the axonal localization of Wnd is not through the local protein synthesis. Excessive Wnd
96 signaling impairs *ppk*-GAL4 activity, compounding our analysis (Wang et al., 2013). Thus, we
97 treated larvae with DLKi/GNE-3511, a specific inhibitor of DLK kinase activity (Patel et al.,
98 2017b). DLKi did not affect larva viability nor basal Cd4a morphology. A kinase-dead version of
99 Wnd, Wnd-KD::GFP showed similar axonal enrichment in the presence and in the absence of
100 DLKi, which further suggests that the axonal localization of Wnd is independent of Wnd kinase
101 activity (**Figure 1C** and **1D**).

102

103 **Wnd protein turnover by Hiw is restricted in the axon terminals.**

104 The protein levels of DLK proteins are highly suppressed by a neuronal ubiquitin ligase
105 PHR1/RPM-1/Hiw in mice, *C elegans*, and *Drosophila* (Nakata et al., 2005; Collins et al., 2006;
106 Xiong et al., 2010; Huntwork-Rodriguez et al., 2013). One possible way of enriching Wnd
107 proteins in axons might be to degrade Wnd in the cell body but not in the axon terminals by Hiw.
108 Our Wnd transgenes showed detectable expression levels in the cell body unlike Wnd-GFSTF,
109 which allowed us to test this possibility. We expressed Wnd-KD::GFP in C4da neurons of wild-
110 type and *hiw* mutant animals. The fluorescent intensity of Wnd-KD::GFP in the cell body and in
111 the axon terminals were directly compared (**Figure 2**). The prediction was that *hiw* mutations
112 would increase Wnd-KD::GFP expression in the cell body, but not in the axon terminals. To our
113 surprise, we did not observe any changes in Wnd-KD::GFP expression levels from the cell body
114 of *hiw* mutant C4da neurons in comparison to those from wild-type control. In contrast, we

115 observed a dramatic 7-fold increase of Wnd-KD::GFP expression levels in the axon terminals by
116 *hiw* mutations (**Figure 2**). The result strongly suggests that Hiw-mediated degradation of Wnd is
117 not responsible for axonal enrichment of Wnd proteins. Rather, this suggests that Wnd proteins
118 are transported towards the axon terminals to be regulated by Hiw. DLK proteins serve as a
119 stress sensor for neuronal stress. To avoid unwanted stress responses, DLK protein levels are
120 constantly suppressed under normal conditions. In this scenario, preventing Wnd transport out
121 of the neuronal cell body will result in deregulated Wnd protein expression levels, which
122 potentially results in exacerbated stress signaling.

123

124 **The protein palmitoylation of Wnd is essential for axonal localization of Wnd.**

125 To test the idea, we sought out the necessary motifs in Wnd protein for axonal transport.
126 *Mi{MIC}wnd*^{GFSF} is recessive lethal, which suggests that the insertion of the GFSF-tag hamper
127 the proper protein folding of Wnd, and that the axonal localization motifs in Wnd may not require
128 fully folded Wnd proteins. Thus, we set out a structure-function analysis of Wnd by serially
129 deleting Wnd transgenes by 100 amino acids (aa) in hope to narrow down the motifs for axonal
130 transport (**Figure 3A**). The Wnd transgenes were expressed in C4da neurons, and Wnd axonal
131 enrichment was measured as in Figure 1. While deleting the first 100 aa of Wnd
132 (WndΔ100::GFP) did not affect the axonal enrichment of Wnd, deleting the first 200aa of Wnd
133 (WndΔ200::GFP) resulted in a dramatic 43-fold reduction in Wnd axonal enrichment. Deleting
134 101-200aa of Wnd (WndΔ101-200::GFP) caused a similar, dramatic reduction in Wnd axonal
135 localization (**Figure 3B**). This suggest that 101-200aa of Wnd contains a motif for axonal
136 transport. Interestingly, Wnd101-200 region contains an evolutionarily conserved palmitoylation
137 motif — Cysteine-130 (Wnd-C130) (**Figure 3C**). The palmitoylation site has been shown to be
138 required for associating DLK to neuronal vesicles and for DLK signaling in mammalian neurons
139 and in *C. elegans* (Holland et al., 2016). However, its role in axonal localization of DLK proteins

140 is not known. Furthermore, whether *Drosophila* DLK, Wnd undergoes protein palmitoylation was
141 not known. To confirm the protein palmitoylation on Wnd-C130, we mutated the Cysteine to
142 Serine and named Wnd-C130S. We expressed a wild-type Wnd (Wnd::GFP) and a
143 palmitoylation site mutated Wnd (Wnd-C130S::GFP) in the cultured *Drosophila* Schneider 2
144 (S2) cells using PEI-mediated transfection (Longo et al., 2013) and performed the Acyl-Biotin
145 Exchange (ABE) assay (Brigidi and Bamji, 2013) to measure protein palmitoylation of Wnd
146 proteins. The result showed about 50% reduction of protein palmitoylation in Wnd-C130S::GFP
147 as compared to Wnd::GFP (**Figure 3D**), which strongly suggests that Wnd-C130 is a
148 palmitoylation site. Next, we expressed Wnd::GFP and Wnd-C130S::GFP in the larval C4da
149 neurons and measured their axonal enrichment. The result showed a dramatic 30-fold reduction
150 in Wnd axonal localization (**Figure 3E**). Taken together, our data demonstrates that Wnd-C130
151 is a palmitoylation site in *Drosophila* and that this palmitoylation is essential for axonal
152 localization of Wnd.

153

154 **dHIP14 is required for Wnd axonal localization**.

155 Next, we asked which palmitoyl-transferase (PAT) is responsible for Wnd axonal localization.
156 DHHC family PATs perform palmitoylation reaction on Cysteine residue. There are twenty-two
157 putative DHHC (PAT) in *Drosophila* (Bannan et al., 2008). A previous work has shown that DLK
158 can be palmitoylated by at least ten DHHC-PATs in a heterologous system (Holland et al.,
159 2016). A more recent work has shown that Zdhhc17/Huntingtin-interacting protein14 (HIP14)
160 mediates DLK palmitoylation on the Golgi complex of rat dorsal root ganglion neurons (Niu et
161 al., 2020). Interestingly, we observed a punctate localization pattern of Wnd-KD::GFP in the
162 larval C4da neurons (**Figure 1** and **2**), which resembles the somatic Golgi in the larval C4da
163 neurons (Zhou et al., 2014). Additionally, the punctate localization pattern of Wnd proteins in the
164 cell body seemed to be well-correlated with axonal localization of truncated Wnd proteins

165 (**Figure 3B**), which suggests that Wnd palmitoylation takes place on the somatic Golgi. To test if
166 somatic Golgi localization is necessary for Wnd axonal localization, we expressed serially
167 deleted Wnd proteins along with a medial-trans Golgi marker, ManII-Tag::RFP (Zhou et al.,
168 2014) and performed a co-localization analysis of Wnd proteins and ManII-Tag::RFP using the
169 Manders Coefficient (Bolte and Cordelières, 2006; Pike et al., 2017) (**Figure 4A**). The results
170 showed a significant colocalization between Wnd-KD::GFP, Wnd-KDΔ100::GFP, and ManII-
171 Tag::RFP. The co-localization requires Wnd101-200aa because Wnd-Δ200::GFP nor Wnd-
172 Δ101-200::GFP showed co-localization with ManII-Tag::RFP. Note that Wnd101-200aa was
173 required for Wnd axonal localization (**Figure 3B**). Taken together, these suggest that Wnd is
174 recruited to somatic Golgi before being transported to the axon terminals, and that somatic
175 Golgi is the site of Wnd palmitoylation. Zdhhc17/HIP14 is known to be localized on Golgi (Niu et
176 al., 2020). We tested if the *Drosophila* ortholog of Zdhhc17/HIP, dHIP14 is present in the
177 somatic Golgi of C4da neurons. We expressed a Tdtomato-tagged dHIP14
178 (dHIP14::Tdtomato)(Stowers and Isacoff, 2007) along with ManII::GFP (Ye et al., 2007) and
179 measured the Pearson coefficient to evaluate the puncta colocalization (Pike et al., 2017). The
180 result showed a strong Golgi localization of dHIP14::Tdtomato in C4da cell bodies (Pearson's
181 coefficient 0.85 ± 0.029, **Figure 4B**). A strong colocalization between dHIP14::Tdtomato and
182 Wnd-KD::GFP was also observed in C4da cell bodies (Pearson's coefficient 0.86 ± 0.039,
183 **Figure 4C**), presumably on the somatic Golgi. We tested a role of dHIP14 by expressing Wnd-
184 KD::GFP in *dHIP14* mutants, *dHIP14* ^{ex11} (Stowers and Isacoff, 2007). The result shows a
185 significant reduction in Wnd axonal localization by *dHIP14* mutations (**Figure 4D**). These
186 suggest that dHIP14 is responsible for axonal localization of Wnd by palmitoylation.

187 **Palmitoylation-defective Wnd exhibits increased protein expression levels.**

188 Next, we reasoned that if axonal localization is a necessary step for Wnd protein turnover, the
189 palmitoylation-defective Wnd or Wnd-C130S would have increased protein expression levels.

190 We expressed Wnd::GFP and Wnd-C130S::GFP under a pan-neuronal driver, *Elav*-GAL4.
191 Overexpressing catalytically active Wnd proteins in the nervous system leads to lethality. Thus,
192 larvae were fed with DLKi. The total Wnd::GFP protein expression levels were measured in the
193 larval brain lysates using Western blot analysis (**Figure 5A**). The result showed a dramatic
194 increase (7-fold) of total Wnd protein levels of Wnd-C130S::GFP as compared to those of
195 Wnd::GFP. To determine the cellular location where Wnd-C130S::GFP expression occurs, we
196 expressed Wnd::GFP and Wnd-C130S::GFP in the larval C4da neurons using *ppk*-GAL4, and
197 directly compared the protein expression levels of the Wnd transgenes in C4da axon terminals
198 and in C4da cell body (**Figure 5B**). While Wnd-C130S::GFP showed reduced protein
199 expression in C4da axon terminals (3-fold reduction) as compared to that of Wnd::GFP, we
200 observed a dramatic 10-fold higher protein expression levels from Wnd-C130S::GFP in C4da
201 cell body in comparison to those of Wnd::GFP. Taken together, these demonstrate that axonal
202 transport out of neuronal cell body is necessary for Wnd to undergo proper protein turnover.

203

204 **A palmitoylation-defective Wnd causes exacerbated neuronal stress responses.**

205 DLK triggers neuronal stress signaling and its activity is mainly regulated by its protein levels
206 (Nakata et al., 2005; Collins et al., 2006; Karney-Grobe et al., 2018). The failure of suppressing
207 Wnd protein levels in Wnd-C130S::GFP may lead to excessive stress signaling in neurons. The
208 palmitoylation of DLK is known to be essential for DLK signaling in *C. elegans* and in
209 mammalian cells (Holland et al., 2016; Martin et al., 2019; Niu et al., 2020, 2022). However, it is
210 not known how the palmitoylation in *Drosophila* DLK/Wnd affects its signaling capacity. Unlike
211 diffuse cytoplasmic expression pattern of palmitoylation-deficient DLK proteins in *C. elegans*
212 and mammalian cells, we observed a discrete subcellular expression pattern of Wnd-
213 C130S::GFP in C4da cell body (**Figure 3E**), which showed a strong colocalization with the
214 somatic Golgi (Data not shown). A recent work from Tortosa et al. suggested that it is

membrane localization of DLK proteins, but not palmitoylation itself is essential for DLK signaling (Tortosa et al., 2022). Thus, we tested whether Wnd-C130S::GFP retains signaling capacity. One of the neuronal events caused by hyperactive Wnd signaling is exuberant axon arborization (Kim et al., 2013). We expressed Wnd-KD::GFP, Wnd::GFP, and Wnd-C130S::GFP in the larval C4da neurons and measured number of connecting fibers in C4da neuropil to evaluate axon arborization (**Figure 5C**). The method was successfully used to estimate axon arborization previously (Wang et al., 2013; Sterne et al., 2015; Singh et al., 2022). Wnd-KD::GFP was used as a negative control. The result showed exuberant axon arborization from the C4da neurons expressing Wnd::GFP and Wnd-C130S::GFP, but not from Wnd-KD::GFP (**Figure 5C** and **5D**). This strongly suggests that unlike DLK proteins from *C. elegans* and mammalian cells, the palmitoylation on Wnd-C130 is not essential for the signaling capacity of Wnd.

DLK-mediated stress signal was shown to cause neuronal loss in multiple neurodegenerative disorder models (Patel et al., 2015, 2017a; Larhammar et al., 2017a; Le Pichon et al., 2017; Niu et al., 2022). Consistently, overexpressing Wnd was shown to induce eye degeneration in *Drosophila* (Ma et al., 2015). We expressed Wnd::GFP, Wnd-C130S::GFP, and Wnd-KD::GFP in *Drosophila* eye using *GMR*-GAL4 (Seong et al., 2001). Expressing Wnd::GFP or Wnd-C130S::GFP caused pupa lethality (Data not shown) suggesting that hyperactive Wnd signaling is toxic to fly development. Thus, we raised flies at a lower temperature to reduce transgene expression. We found that the flies expressing Wnd::GFP or Wnd-C130S::GFP exhibited severe eye degeneration phenotypes while Wnd-KD::GFP did not affect eye development (**Figure 6A**). To quantify severity of eye degeneration phenotypes, we measured the area of the degenerated eye. The result showed significantly smaller eye area from Wnd-C130S::GFP expression as compared to those from Wnd::GFP (**Figure 6B**), which suggests that Wnd-C130S::GFP triggered excessive stress signaling because of its deregulated protein turnover.

240 Discussion

241 Here, we report a novel coupling of axonal DLK protein expression and protein turnover in
242 neuronal stress signaling. We demonstrate that the protein turnover of *Drosophila* DLK, Wnd is
243 confined in axons, and that a failure to localize Wnd proteins in axons leads to deregulated Wnd
244 protein turnover, hence increased protein levels. The excessive neuronal stress responses
245 caused by the latter underscore the importance of DLK protein transport and localized protein
246 turnover.

247 Many neuronal proteins exhibit polarized protein expression patterns. DLK proteins are found in
248 the axonal compartments of diverse animals (Xiong et al., 2010; Klinedinst et al., 2013; Holland
249 et al., 2016; Niu et al., 2020, 2022). However, the extent of DLK axonal localization was not
250 studied in depth, presumably because of technical limitations. We employed *Drosophila* larval
251 sensory neurons to answer this question. Our data suggests that Wnd proteins are highly
252 enriched in the axon terminals of these neurons (**Figure 1**). Given that Wnd encodes a
253 cytoplasmic protein, the extent of axonal enrichment was rather surprising. Wnd protein levels
254 are constantly suppressed by Hiw in the axon terminals. Without such suppression, Wnd
255 proteins would show well over 70-fold enrichment in axons, which might be on par with those of
256 synaptic proteins. The UTRs of *wnd* are dispensable for Wnd axonal enrichment (**Figure 1B**),
257 which suggests that Wnd protein transport is responsible for such axonal enrichment of Wnd.
258 Consistent with the notion, Wnd proteins were found on the antero- and retrograde moving
259 vesicles in axons (Xiong et al., 2010; Holland et al., 2016; Li et al., 2017). Together, these
260 suggest that Wnd proteins are synthesized in the neuronal cell body and transported into axons
261 by a highly active and efficient anterograde transport process.

262 What might be such a transport mechanism? DLK genes encode cytoplasmic proteins. Protein
263 palmitoylation is reported as an important post-translational mechanism for protein transport
264 (Aicart-Ramos et al., 2011; Tortosa and Hoogenraad, 2018). It increases hydrophobicity of

265 target proteins to aid membrane association so that palmitoylated proteins are transported along
266 with the membrane vesicles they associate. We found that protein palmitoylation on Wnd-C130
267 is essential for Wnd axonal localization. Interestingly, the palmitoylation defective Wnd-C130S
268 exhibited large punctate structures in the cell body (**Figure 3E**) that were co-localized with
269 somatic Golgi complex (Data not shown). This suggests that Wnd-C130 palmitoylation is not
270 essential for membrane association. The residual palmitoylation that we observed in Wnd-
271 C130S (**Figure 3D**) may indicate the presence of a second palmitoylation site and may explain
272 how Wnd-C130S associates with the Golgi. Consistent with this idea, DLK proteins in
273 mammalian cells and *C. elegans* are palmitoylated on a single Cysteine residue and showed
274 diffuse cytoplasmic expression when the cysteine residue was mutated (Holland et al., 2016).
275 This raises a question of why Wnd-C130S::GFP is not transported to axons with this remaining
276 palmitoylation and membrane association. Interestingly, a recent study proposed the role of
277 protein palmitoylation in the anterograde transport in the Golgi complex (Ernst et al., 2018). We
278 show that a Golgi-localized PAT, dHIP14 is required for Wnd axonal localization (**Figure 4**). We
279 envision that Wnd-C130 palmitoylation is a necessary step towards the axonal anterograde
280 transport from the somatic Golgi complex rather than merely acting as a membrane anchor.
281 Future studies will be needed to unveil neuronal protein transport pathways of DLK proteins.

282 Why does DLK need to be transported into axons? Our study of the palmitoylation-defective
283 Wnd provides an insight. DLK proteins act as an axonal stress sensor (Asghari Adib et al.,
284 2018; Farley and Watkins, 2018). In this model, DLK protein levels or activity increases by
285 axonal stress followed by DLK-mediated axonal retrograde signaling. This model is supported
286 by various studies. For example, the expression levels of GFP::Wnd-KD were increased in the
287 proximal axons after a nerve injury in *Drosophila* larval motor neurons (Xiong et al., 2010). DLK
288 mediates STAT3 retrograde signaling after axon injury in mouse sensory neurons (Shin et al.,
289 2012). The local application of DLK inhibitors in axons prevented stress signaling caused by

290 trophic factor deprivation in compartmentalized dorsal root ganglion explant culture (Larhammar
291 et al., 2017b). Collaborating with the studies showing the requirement of DLK palmitoylation in
292 axonal vesicle association and neuronal stress response (Holland et al., 2016; Martin et al.,
293 2019; Niu et al., 2020, 2022), these led to a model in which DLK signaling requires axonal
294 expression of DLK proteins (Asghari Adib et al., 2018). Our study suggests that this may not
295 represent a complete picture. Although expression levels of Wnd-C130S is significantly reduced
296 in axons, it did show similar in axon arborization (**Figure 5**) or even greater stress responses
297 and in neuronal loss (**Figure 6**). In fact, it is the total expression levels of Wnd that showed a
298 correlation with the eye loss phenotypes. Thus, our study suggests that DLK axonal localization
299 is not a prerequisite for DLK signaling, and that DLK retrograde pathway is a way employed by
300 axonally expressed DLK. Consistent with this notion, a recent work demonstrated that DLK
301 palmitoylation is not essential for DLK signaling but its main role is to bring DLK proteins to the
302 intracellular membrane (Tortosa et al., 2022).

303 Our study shows that Hiw-mediated Wnd protein turnover is restricted in axons. How does Hiw
304 perform such compartmentalized Wnd targeting? One possibility is that Hiw is only present in
305 the axon terminals, not in the cell body. Phr1 was shown to be expressed in axonal segments of
306 motor neuron explants and in the axon shaft of sensory neurons but was low or absent in the
307 growth cone (Lewcock et al., 2007) although it is not known whether and how much Phr1
308 proteins are present in the cell body. Unfortunately, the lack of immunostaining compatible Hiw
309 antibody preclude us from testing the possibility. However, although present in axons,
310 transgenic expression of Hiw, GFP::Hiw showed a significantly higher expression in the motor
311 neuron cell body (Xiong et al., 2010). Moreover, a study has shown that Hiw controls dNMNAT2
312 expression both in the cell body and the neuromuscular junction (Xiong et al., 2012). Together,
313 it is unlikely that Hiw protein expression itself is restricted in the axon terminals. Another
314 possibility is that DLK proteins are protected from PHR1/RMP-1/Hiw in the cell body.

315 Interestingly, DLK protein stability can be enhanced by Hsp90 (Karney-Grobe et al., 2018),
316 protein phosphorylation by JNK (Huntwork-Rodriguez et al., 2013), and PKA (Hao et al., 2016).
317 It will be interesting to see how these protective pathways collaborate with PHR1/RMP-1/Hiw to
318 execute axon-specific protein turnover of DLK proteins.

319 We propose the novel coupling between axonal transport and protein turnover of DLK proteins.
320 What might be the biological role of this coupling? Recent studies suggest that DLK is a central
321 player in neuronal death including Alzheimer's disease and amyotrophic lateral sclerosis
322 (Pozniak et al., 2013; Welsbie et al., 2013, 2017; Larhammar et al., 2017a, 2017b; Le Pichon et
323 al., 2017; Patel et al., 2017a), which suggests that DLK activity or protein levels might be
324 deregulated in these conditions. Interestingly, defective axonal transport is an early hallmark in
325 many neurodegenerative disorders (Chevalier-Larsen and Holzbaur, 2006; De Vos et al., 2008;
326 Guo et al., 2020). The defective axonal transport in these neurodegenerative conditions might
327 lead to accumulation of DLK in the cell body and deregulated DLK protein levels. It is tempting
328 to envision that defective anterograde transport and subsequent accumulation of DLK proteins
329 in neuronal cell bodies is causative of neuronal loss in these neurodegenerative diseases.
330 Interestingly, increased DLK protein levels were reported in neuronal cell bodies after neuronal
331 insults (Watkins et al., 2013; Welsbie et al., 2013). It is also interesting to note that DLK
332 signaling is activated by cytoskeletal disruptions (Valakh et al., 2013, 2015), which might disrupt
333 cytoskeleton-based axonal transport. The possibility is highly intriguing and will be an important
334 future direction to investigate.

335 Taken together, our study demonstrates a novel coupling between axonal protein localization
336 and protein turnover and provides an insight on the potential link between defective axonal
337 transport in neurodegenerative disorders and DLK-mediated stress signaling.

Acknowledgments

We thank Drs. Steve Stowers and Catherine Collins for sharing reagents. Research reported in this study used the Cellular and Molecular Imaging Core facility at the University of Nevada Reno, which was supported by NIH GM103650. This study was supported by NIH R01NS116463 and P20GM103440 (NV INBRE) to J.K. The content is solely the responsibility of the authors and does not necessarily represent the official views of the National Institutes of Health.

Author contributions

S.K., Y.Q., M.S., and J.K. designed the experiments. S.K., Y.Q., M.S., and J.K. performed experiments. S.K. and J.K. wrote the manuscript.

Declaration of interests

The authors declare no competing financial interests.

352 Figure legends

353 **Figure 1. Wnd is highly enriched in the axon terminals of *Drosophila* sensory neurons.**

354 (A) A representative image of *Mi{MIC}wnd*^{GFSTF} in the neuropil of larval ventral nerve cords (top)
355 and C4da neuron cell body (bottom) from a hemizygous *hiw* mutant (*hiw*$^{\triangle N}$) were shown. Wnd-
356 GFP (Wnd-GFSTF, green) and anti-HRP staining (magenta). Scale bar = 10 μm.

357 (B) The Wnd::GFP (with or without *wnd*-UTRs, green) along with mCD8::RFP (magenta) were
358 expressed in the larval C4da neurons in the presence of DLK inhibitor (DLKi). The expression
359 levels of transgenes were shown in C4da cell body and the axon terminals. Scale bar = 10 μm.

360 (C) A Wnd kinase-dead (Wnd-KD::GFP, green) along with mCD8::RFP (magenta) were
361 expressed in the larval C4da neurons in either regular food or food containing DMSO (vehicle
362 control) or DLKi. The expression levels of transgenes were shown in C4da cell body and the
363 axon terminals. Scale bar = 10 μm.

364 (D) The axonal enrichment index from (B) and (C) were expressed as median ± 95% CI.
365 Sample numbers were 5'UTR-Wnd::GFP-3'UTR (*w*^{1118}*; UAS-5'UTR-Wnd::GFP-3'UTR/+;ppk-*
366 *GAL4, UAS-mCD8::RFP/+*) with DLKi (n = 26), Wnd::GFP (*w*^{1118}*; UAS-Wnd::GFP-SV40 3'UTR*
367 */+; ppk-GAL4, UAS-mCD8::RFP/+*) with DLKi (n = 22), Wnd-KD::GFP (*w*^{1118}*; UAS-Wnd-*
368 *KD::GFP/+; ppk-GAL4, UAS-mCD8::RFP/+*) (n = 10), with DLKi (n = 6), with DMSO (n = 6);
369 One-way ANOVA ($F_{(4,65)}$ = 1.017) followed by post hoc Tukey's multiple comparison test.

370 **Figure 2. Highwire regulation of Wnd is restricted in the axon terminals.**

371 The Wnd-KD::GFP along with mCD8::RFP (magenta) were expressed in C4da neurons in wild-
372 type, *wt* (*w^{1118};UAS-Wnd-KD::GFP/+;ppk-Gal4, UAS-mCD8::RFP/*+) or in *hiw* mutant (*$hiw^{\Delta N}$;*
373 *UAS-Wnd-KD::GFP/+;ppk-Gal4,UAS-mCD8::RFP/*+) larvae. Representative images of Wnd-
374 KD::GFP and mCD8::RFP in C4da cell bodies and axon terminals, stained for anti-GFP (green)
375 and anti-RFP (magenta). The average Wnd-KD::GFP intensity from cell bodies and axon
376 terminals were quantified and expressed as median ± 95% CI (Cell body: n = 8, U=25,
377 P=0.3213, Axon terminal : n = 9, U=0, P<0.0001, two-tailed Mann-Whitney test). The images of
378 mCD8::RFP were shown as counter staining. Scale bar = 10 μm.

379 **Figure 3. Wnd palmitoylation is required for Wnd axonal localization.**

380 (A) Schematic of Wnd deletion mutants. Deletion of the N-terminal 1-100 aa of Wnd (WndΔ100),
381 Deletion of the N-terminal 1-200 aa of Wnd (WndΔ200), and Deletion of the N-terminal 101-200
382 aa of Wnd (WndΔ101-200).

383 (B) The transgenes of serially deleted Wnd (green) along with mCD8::RFP were expressed in
384 the larval C4da neurons. Note that WndΔ100 was further mutated to remove kinase activity
385 (Wnd-KDΔ100). The expression levels of Wnd::GFP proteins in C4da cell body and the axon
386 terminals were shown (left). Scale bars = 10 μm. The axonal enrichment of each Wnd
387 transgenes were measured using mCD8::RFP as a normalization control (right) and expressed
388 as median ± 95% CI. One-way ANOVA ($F_{(3,59)}$ = 103.8) followed by post hoc Tukey's multiple
389 comparison test. The p values from Tukey's test are indicated in the graph. Genotypes were
390 Wnd-KDΔ100 (*UAS-Wnd-KDΔ100-KD::GFP/+;ppk-Gal4, UAS-mCD8::RFP/+*), WndΔ200 (*UAS-*
391 *WndΔ200::GFP/+;ppk-Gal4, UAS-mCD8::RFP/+*), and WndΔ101-200 (*UAS-WndΔ101-*
392 *200::GFP/+;ppk-Gal4, UAS-mCD8::RFP/+*).

393 (C) Wnd-C130 is an evolutionarily conserved palmitoylation site.

394 (D) The Acyl Biotin Exchange (ABE) assay was performed on the beads coupled with Wnd
395 proteins that were expressed in S2 cells. Wnd-C130S::GFP is a palmitoylation defective version
396 of Wnd. "No HAM" serves as a negative control since Biotin exchange does not occur in the
397 absence of HAM. Biotin blot shows protein palmitoylation levels while total Wnd shows Wnd
398 protein levels in the pulldown. The numbers indicate the relative amount of palmitoylated Wnd in
399 Wnd::GFP and Wnd-C130S::GFP.

400 (E) Wild-type Wnd::GFP transgene (Wnd::GFP) and palmitoylation defective Wnd transgenes
401 (Wnd-C130S::GFP) along with mCD8::RFP were expressed in the larval C4da neurons in the
402 presence of DLKi. The expression levels of Wnd::GFP proteins in C4da cell body and the axon

403 terminals were shown (top). Scale bar = 10 μm. The axonal enrichment of the Wnd transgenes
404 were measured using mCD8::RFP as a normalization control (bottom) and expressed as
405 median ± 95% CI (n = 12 for Wnd::GFP, n = 10 for Wnd-C130S::GFP, Mann-Whitney U=0,
406 P<0.0001, two-tailed Mann-Whitney test). Genotypes were Wnd::GFP (*UAS-Wnd::GFP/+;ppk-*
407 *Gal4, UAS-mCD8::RFP/+*) and Wnd-C130S::GFP (*UAS-WndC130S::GFP/+;ppk-Gal4, UAS-*
408 *mCD8::RFP/+*).

409 **Figure 4. dHIP14 is required for Wnd axonal localization.**

410 (A) Wnd transgenes (green) along with a Golgi marker, ManII-Tag::RFP (magenta) were
411 expressed in the larval C4da neurons. The expression patterns of the two transgenes in C4da
412 cell bodies were shown (left). Scale bar = 5 μm. The Manders' overlap coefficient between Wnd
413 transgenes and ManII-Tag::RFP was measured and expressed as median ± 95% CI (right).
414 Genotypes and sample numbers were Wnd-KD::GFP (*w^{1118}; UAS-Wnd-KD::GFP/+;ppk-*
415 *GAL4/UAS-ManII-Tag-RFP*, n = 23), Wnd-KD∆100::GFP (*w^{1118}; UAS-Wnd-∆100-*
416 *KD::GFP/+;ppk-GAL4/UAS-ManII-Tag-RFP*, n=26), Wnd-∆200::GFP (*w^{1118}; UAS-Wnd-*
417 *∆200::GFP/+;ppk-GAL4/UAS-ManII-Tag-RFP*, n = 28) and Wnd-∆101-200::GFP (*w^{1118}; UAS-*
418 *Wnd∆101-200::GFP/+;ppk-GAL4/UAS-ManII-Tag-RFP*, n = 15). One-way ANOVA ($F_{(3,88)}$ =
419 129.8) followed by post hoc Tukey's multiple comparison test. The p values from Tukey's test
420 are indicated in the graph.

421 (B) A Golgi marker, ManII::GFP (green) was expressed in the larval C4da neurons along with
422 dHIP14::Tdtomato (magenta). The image was taken from a C4da cell body. Scale bar = 10 μm.

423 (C) Wnd-KD::GFP (green) was expressed in the larval C4da neurons along with
424 dHIP14::Tdtomato (magenta). The image was taken from a C4da cell body. Scale bar = 10 μm.

425 (D) Wnd-KD::GFP (green) along with mCD8::RFP (magenta) were expressed in the larval C4da
426 neurons from wild-type (*wt*) or from homozygous *dHIP14* mutants (*dHIP14 ^{ex11}*). Scale bar = 10
427 μm. The axonal enrichment of Wnd-KD::GFP was measured and expressed as median ± 95%
428 CI (Mann-Whitney U=13, P<0.0001, two-tailed Mann-Whitney test). Genotypes and sample
429 numbers were *wt* (*UAS-Wnd-KD::GFP/ppk-Gal4, U-mCD8::RFP;+/+*, n = 17) and *dHIP14 ^{ex11}*
430 (*UAS-Wnd-KD::GFP/ppk-Gal4, U-mCD8::RFP;dHIP14^{ex11}*, n = 16).

431 **Figure 5. Increased protein expression levels of palmitoylation-defective Wnd.**

432 (A) Wnd::GFP and Wnd-C130S::GFP were expressed in the larval nervous system using a pan
433 neuronal driver in the presence of DLKi. Larval brain lysates were subjected to Western blot
434 analysis using a GFP antibody. Elav blot was used as a loading control. The GFP blots were
435 normalized by Elav blots and expressed as mean ± SEM (n = 4, t = 9.409, df =3, p=0.0025, two-
436 tailed ratio paired t-test). Genotypes were Wnd::GFP (*elav-Gal4/+; UAS-Wnd::GFP/+;*) and
437 WndC130S::GFP (*elav-Gal4/+; UAS-WndC130S::GFP/+;*).

438 (B) Wnd transgenes (green) along with mCD8::RFP were expressed in the larval C4da neurons
439 to directly compare the expression levels of Wnd::GFP and Wnd-C130S::GFP in C4da cell
440 bodies and axon terminals. The larvae were treated with DLKi. Scale bar = 10 μm. The average
441 fluorescent intensities from GFP staining of each larva sample were measured and expressed
442 as median ± 95% CI (Axon terminal: Mann-Whitney U=2, P=0.0162, two-tailed Mann-Whitney
443 test, Cell body: Mann-Whitney U=0, P<0.0001, two-tailed Mann-Whitney test). Genotypes and
444 sample numbers were Wnd::GFP (*UAS-Wnd::GFP/+;ppk-Gal4, UAS-mCD8::RFP/+*, n = 8) and
445 Wnd-C130S::GFP (*UAS-WndC130S::GFP/+;ppk-Gal4, UAS-mCD8::RFP/+*, n = 4).

446 (C) Wnd transgenes along with mCD8::RFP were expressed in the larval C4da neurons. The
447 axon terminal morphology was visualized by mCD8::RFP. Note the increased number of
448 connecting fibers between neuropils. Wnd-KD::GFP (*UAS-Wnd-KD::GFP/+;ppk-Gal4, UAS-*
449 *mCD8::RFP/+*), Wnd::GFP(*UAS-Wnd::GFP/+;ppk-Gal4, UAS-mCD8::RFP/+*), and
450 WndC130S::GFP (*UAS-WndC130S::GFP/+;ppk-Gal4, UAS-mCD8::RFP/+*). Scale bar = 10 μm.

451 (D) The number of connecting fibers between neuropils was measured and expressed as
452 median ± 95% CI. One-way ANOVA ($F_{(2, 27)}$ = 31.84) followed by post hoc Tukey's multiple
453 comparison test. The p values from Tukey's test are indicated in the graph. Sample numbers
454 are 10 for all genotypes.

455 **Figure 6. Palmitoylation-defective Wnd caused exacerbated neuronal loss.**

456 (A) Representative images of fly eye phenotypes from Wnd::GFP fly (Wnd::GFP), a fly
457 expressing Wnd::GFP under GMR-GAL4 (GMR>Wnd::GFP), a fly expressing Wnd-C130S::GFP
458 under GMR-GAL4 (GMR>Wnd-C130::GFP), and a fly expressing Wnd-KD::GFP under GMR-
459 GAL4 (GMR>Wnd-KD::GFP).

460 (B) Eye area was quantified from the genotypes and expressed as median ± 95% CI. One-way
461 ANOVA ($F_{(6, 136)} = 362.0$) followed by post hoc Tukey's multiple comparison test. The p values
462 from Tukey's test are indicated in the graph. Genotypes and sample numbers were GMR
463 *(;GMR-GAL4/+*;, n = 21), Wnd::GFP (;*UAS-Wnd::GFP/+;,* n = 22), Wnd-C130S::GFP (;*UAS-*
464 *Wnd-C130S::GFP/+;, n = 20*), Wnd-KD::GFP (;*UAS-Wnd-KD::GFP/+;, n = 24*), GMR>Wnd::GFP
465 (*;GMR-GAL4/UAS-Wnd::GFP; n = 17*), GMR>Wnd-C130S::GFP (*;GMR-GAL4/UAS-Wnd-*
466 *C130S::GFP; n = 16*), and GMR>Wnd-KD::GFP ((*;GMR-GAL4/UAS-Wnd-KD::GFP; n = 23*).
467 Note a more severe eye phenotypes in GMR>Wnd-C130S::GFP as compared to
468 GMR>Wnd::GFP.

469 Experimental Procedures

470 **Drosophila Strains, rearing, DNA Constructs for Generating Transgenic Flies**

471 The following *Drosophila* strains were reared at 25°C in a humidified chamber. *ppk-GAL4*
472 (Grueber et al., 2007); *UAS-dHIP14::Tdtomato* and *dHIP14*^{ex11} (Stowers and Isacoff, 2007);
473 *hiw*$^{\Delta N}$ (Wu et al., 2005); *UAS-ManII::GFP* (Ye et al., 2007); *UAS-ManII-Tag::RFP* (Zhou et al.,
474 2014); *Mi{MIC}wnd* ^{GFSTF} (Venken et al., 2011); *GMR-Gal4* (Seong et al., 2001); *elav-Gal4*^{C155}
475 (BDSC #459); *w*^{1118} (BDSC #3605).

476 To generate DNA constructs of *Wnd* with its natural 5'- and 3'-UTRs and the serial deletion
477 constructs of Wnd, the genomic sequences of the 5'-UTR and 3'-UTR of *Wnd* were obtained
478 from *w*^{1118} genomic DNA by PCR. The coding sequence of *Wnd* was recovered from UAS-Wnd
479 (Collins et al., 2006) via PCR and inserted into the pUASTattB plasmid using NotI and XbaI
480 restriction sites. UAS-Wnd-KD::GFP and Wnd-KD∆100 were generated by site-directed
481 mutagenesis using In-Fusion® Snap Assembly Master Mix (Takara Bio USA, Inc, San Jose,
482 CA). UAS-WndC130S::GFP and UAS-Wnd∆101-200::GFP were generated by site-directed
483 mutagenesis. The resulting PCR product was ligated using a Q5® Site-Directed Mutagenesis
484 Kit (New England BioLabs, Ipswich, MA) following instructions of the manufacturer.

485 Transgenic flies were generated by PhiC31-mediated germline transformation using an identical
486 landing site (Bischof et al., 2007).

487 To dose larvae with DLKi (GNE-3511**,** Sigma, St. Louis, MO), DLKi was dissolved in DMSO and
488 was added to a final concentration of 35 μM in fly food. Fly larvae were raised directly on either
489 control (DMSO) or DLKi containing food.

490 **Drosophila Schneider 2 cell culture, transfection, Palmitoylation assay, and Western blot.**

491 *Drosophil*a Schneider 2 (S2) cells were prepared as previously described (Singh et al., 2022).
492 Cells were transfected with indicated DNA constructs and tubulin-Gal4 (Lee and Luo, 1999)
493 using polyethyleneimine (Polysciences, Warrington, PA) (Longo et al., 2013).

494 Two days after transfection, the Acyl-Biotin Exchange (ABE) assay was performed as modified
495 from Brigidi and Bamji (Brigidi and Bamji, 2013). Cells were lysed in the ice-cold Lysis buffer
496 (LB, 50 mM HEPES/pH 7.4, 150 mM NaCl, 1 mM EDTA, 1% NP40, 5% glycerol, 1 mM PMSF, 1
497 mM Na_3VO_4, 5 mM NaF) with Halt™ protease inhibitor cocktail EDTA- free (ThermoFisher
498 Scientific, Waltham, MA) and 25mM N-ethylmaleimide (Sigma, St. Louis, MO), incubated for 1hr
499 at 4˚C and centrifuged at 1000 xg for 5 min. The resulting post-nuclear lysates were centrifuged
500 at 20,000 xg for 30 min at 4˚C. The supernatant was incubated with the GFP selector (NanoTag
501 Biotechnologies, Göttingen, Germany) for 2 hr at 4˚C to pulldown Wnd-GFP proteins. The GFP
502 selector beads along with bound proteins were recovered by a brief centrifugation and washed
503 two times with LB containing 0.1% SDS before incubating with 1 M hydroxylamine hydrochloride
504 (HAM, Sigma, St. Louis, MO) in LB (pH 7.2) at room temperature for 1 hr. Half of the protein-
505 bound GFP selector beads were incubated with LB without HAM and used as a "-HAM" control.
506 Then, the protein GFP selector beads were washed with pH 6.2 LB twice and treated with 1.6
507 μM EZ-Link™ BMCC-Biotin (ThermoFisher Scientific, Waltham, MA) in pH 6.2 LB for 45 min at
508 4˚C. Beads were washed twice with LB without NP40 before being processed for SDS-PAGE.
509 Proteins were separated by SDS-PAGE and were subjected to Western blot analysis with
510 mouse monoclonal anti-Biotin antibody (Jackson Immunoresearch, West Grove, PA) and
511 chicken polyclonal anti-GFP antibody (Aves Labs, Tigard, OR). The small aliquots of bead
512 samples were blotted using anti-Wnd antibody (Collins et al., 2006) to estimate total Wnd
513 proteins on the beads.

514 To measure Wnd expression in the larval brains, larvae were grown on fly food containing 35
515 μM DLKi food at 20°C in a humidified chamber. The larval central nervous system (the ventral

516 nerve cord and brain lobes) was dissected out from the 3rd instar larvae and collected in ice-cold
517 PBS before recovery by a brief centrifugation at 4°C. The total brain lysates were prepared by
518 directly adding SDS-PAGE sample buffer and homogenization before being resolved on 8%
519 SDS-PAGE gel and subsequent Western blot analysis.

520 **Immunostaining and Imaging**

521 *Drosophila* 3rd instar larvae were prepared for immunostaining as previously described (Singh et
522 al., 2022). Primary antibodies used were rabbit polyclonal anti-RFP (Rockland
523 Immunochemicals, Limerick, PA), chicken polyclonal anti-GFP (Aves Labs, Tigard, OR), and
524 goat anti-horseradish peroxidase conjugated with Cy5 (Jackson ImmunoResearch, West Grove,
525 PA). The secondary antibodies used were Cy2- or Cy5-conjugated goat anti-chicken and Cy2-
526 or Cy5-conjugated goat anti-Rabbit (Jackson ImmunoResearch, West Grove, PA).

527 Confocal imaging was done with a Leica SP8 confocal system, or a custom-built spinning disk
528 confocal microscope equipped with a 63x oil-immersion objective with a 0.3 μm step-sizes.

529 For Wnd axonal enrichment analysis, the C4da neuron cell bodies from abdominal segments 4-
530 6 and the corresponding segments in the ventral nerve cord were imaged. The resulting 3D
531 images were projected into 2D images using a maximum projection method in the imageJ
532 software. A region of interest was drawn in the cell body of C4da neurons, and the mean
533 fluorescence intensity was measured using ImageJ software. The mean fluorescence intensity
534 of UAS-mCD8::mRFP transgene expression was measured from the same region of interest
535 and used as a normalization control. The mean intensities of the C4da cell bodies from a single
536 larva were averaged out to calculate the axonal enrichment index. The axonal enrichment index
537 was defined as Wnd expression (mean intensity) in the axon terminals divided by an average
538 Wnd expression in cell bodies (mean intensity).

539 For Golgi and Wnd colocalization, the Manders' Overlap Coefficient (Pike et al., 2017) was
540 measured as the percentage of total GFP signal overlapping with RFP signal using the ImageJ
541 plugin, JACoP (Bolte and Cordelières, 2006). To analyze puncta colocalization, we used the
542 Pearson coefficient (Pike et al., 2017) that is correlation between each channel signal using
543 JACop.

544 **Axon arborization analysis**

545 The quantitation of axon arborization by counting the axonal connecting fibers (Sterne et al.,
546 2015) were done as previously described.

547 **Drosophila eye degeneration**

548 Flies were raised at 18°C. The flies that are 24 – 48 hr after eclosion were imaged using the
549 Basler ace acA2440-75 µm CCD-camera installed on a stereomicroscope. The region of interest
550 was drawn on the fly eye area from the images and expressed as pixel numbers.

551 **Experimental design and statistical analysis.**

552 All statistical analysis was performed as two-tailed using GraphPad Prism software version
553 7.04. The Mann–Whitney test was used for immunostaining results. A ratio paired t-test was
554 used for Western blot analysis (see Figs. 5A). For multigroup comparisons, one-way ANOVA
555 was used followed by post hoc Tukey's multiple comparisons tests. A p-value smaller than 0.05
556 was considered statistically significant. All p values are indicated as NS; non-significant, *; $P < 0.05$, **; $P < 0.01$, ***; $P < 0.001$, and ****; $P < 0.0001$
557

Oligonucleotides used in this study	SOURCE
5'UTR-Wnd::GFP-3'UTR	This paper
Forward : AGGGAATTGGGAATTTTGGTCGGAATAAACGCG	
Reverse : TAGTGGATCTCTAGAAGCGTTCTTACAAGTTTTCATTTTATTATTAT	
Wnd::GFP	This paper
Forward : GTGCGGCCGCATGCAACCGTTCAGCGAC	
Reverse : CGTCTAGATTACTTGTACAGCTCGTCCATGC	
Wnd-KD::GFP(WndK188A::GFP)	This paper
Forward : GGCGGTCGCGAAGGTGAAGGAGCTGAAGG	
Reverse : ACCTTCGCGACCGCCACAGTCTCGTTC	
Wnd-KD∆100::GFP	This paper
Forward : GGCGGTCGCGAAGGTGAAGGAGCTGAAGG	
Reverse : ACCTTCGCGACCGCCACAGTCTCGTTC	
Wnd∆100::GFP	This paper
Forward : GTGCGGCCGCATGCAGCGCTGGCCACCTCATG	
Reverse : CGTCTAGATTACTTGTACAGCTCGTCCATGC	
Wnd∆200::GFP	This paper
Forward : GTGCGGCCGCATGCTCAGGAAGCTCGATCATGAG	
Reverse : CGTCTAGATTACTTGTACAGCTCGTCCATGC	
WndC130S::GFP	This paper
Forward : CTGCTCGGATCCATGAAGCCC	
Reverse : TCCGTACATCCAGCCAATGGG	
Wnd∆101-200::GFP	This paper
Forward : CTCAGGAAGCTCGATCATGAGAAC	
Reverse : TTGGCACGTGTTTTCCGCACTGC	

558 References

559 Aicart-Ramos, C., Valero, R.A., and Rodriguez-Crespo, I. (2011). Protein palmitoylation and
560 subcellular trafficking. Biochim Biophys Acta 1808, 2981-2994. 10.1016/j.bbamem.2011.07.009.

561 Asghari Adib, E., Smithson, L.J., and Collins, C.A. (2018). An axonal stress response pathway:
562 degenerative and regenerative signaling by DLK. Curr Opin Neurobiol 53, 110-119.
563 10.1016/j.conb.2018.07.002.

564 Bannan, B.A., Van Etten, J., Kohler, J.A., Tsoi, Y., Hansen, N.M., Sigmon, S., Fowler, E., Buff,
565 H., Williams, T.S., Ault, J.G., et al. (2008). The Drosophila protein palmitoylome: characterizing
566 palmitoyl-thioesterases and DHHC palmitoyl-transferases. Fly (Austin) 2, 198-214.
567 10.4161/fly.6621.

568 Bischof, J., Maeda, R.K., Hediger, M., Karch, F., and Basler, K. (2007). An optimized transgenesis
569 system for Drosophila using germ-line-specific phiC31 integrases. Proc Natl Acad Sci U S A 104,
570 3312-3317. 10.1073/pnas.0611511104.

571 Bolte, S., and Cordelières, F.P. (2006). A guided tour into subcellular colocalization analysis in
572 light microscopy. J Microsc 224, 213-232. 10.1111/j.1365-2818.2006.01706.x.

573 Brigidi, G.S., and Bamji, S.X. (2013). Detection of protein palmitoylation in cultured hippocampal
574 neurons by immunoprecipitation and acyl-biotin exchange (ABE). J Vis Exp. 10.3791/50031.

575 Calkins, M.J., Manczak, M., Mao, P., Shirendeb, U., and Reddy, P.H. (2011). Impaired
576 mitochondrial biogenesis, defective axonal transport of mitochondria, abnormal mitochondrial
577 dynamics and synaptic degeneration in a mouse model of Alzheimer's disease. Hum Mol Genet
578 20, 4515-4529. 10.1093/hmg/ddr381.

579 Chevalier-Larsen, E., and Holzbaur, E.L. (2006). Axonal transport and neurodegenerative
580 disease. Biochim Biophys Acta 1762, 1094-1108. 10.1016/j.bbadis.2006.04.002.

581 Chu, Y., Morfini, G.A., Langhamer, L.B., He, Y., Brady, S.T., and Kordower, J.H. (2012).
582 Alterations in axonal transport motor proteins in sporadic and experimental Parkinson's disease.
583 Brain 135, 2058-2073. 10.1093/brain/aws133.

584 Collard, J.F., Côté, F., and Julien, J.P. (1995). Defective axonal transport in a transgenic mouse
585 model of amyotrophic lateral sclerosis. Nature 375, 61-64. 10.1038/375061a0.

586 Collins, C.A., Wairkar, Y.P., Johnson, S.L., and DiAntonio, A. (2006). Highwire restrains synaptic
587 growth by attenuating a MAP kinase signal. Neuron 51, 57-69. 10.1016/j.neuron.2006.05.026.

588 De Vos, K.J., Grierson, A.J., Ackerley, S., and Miller, C.C. (2008). Role of axonal transport in
589 neurodegenerative diseases. Annu Rev Neurosci 31, 151-173.
590 10.1146/annurev.neuro.31.061307.090711.

591 De Vos, K.J., and Hafezparast, M. (2017). Neurobiology of axonal transport defects in motor
592 neuron diseases: Opportunities for translational research? Neurobiol Dis 105, 283-299.
593 10.1016/j.nbd.2017.02.004.

594 Ernst, A.M., Syed, S.A., Zaki, O., Bottanelli, F., Zheng, H., Hacke, M., Xi, Z., Rivera-Molina, F.,
595 Graham, M., Rebane, A.A., et al. (2018). S-Palmitoylation Sorts Membrane Cargo for Anterograde
596 Transport in the Golgi. Dev Cell 47, 479-493.e477. 10.1016/j.devcel.2018.10.024.

597 Farley, M.M., and Watkins, T.A. (2018). Intrinsic Neuronal Stress Response Pathways in Injury
598 and Disease. Annu Rev Pathol 13, 93-116. 10.1146/annurev-pathol-012414-040354.

599 Grueber, W.B., Ye, B., Yang, C.H., Younger, S., Borden, K., Jan, L.Y., and Jan, Y.N. (2007).
600 Projections of Drosophila multidendritic neurons in the central nervous system: links with
601 peripheral dendrite morphology. Development 134, 55-64. 10.1242/dev.02666.

602 Guedes-Dias, P., and Holzbaur, E.L.F. (2019). Axonal transport: Driving synaptic function.
603 Science 366. 10.1126/science.aaw9997.

604 Guillaud, L., El-Agamy, S.E., Otsuki, M., and Terenzio, M. (2020). Anterograde Axonal Transport
605 in Neuronal Homeostasis and Disease. Front Mol Neurosci 13, 556175.
606 10.3389/fnmol.2020.556175.

607 Guo, W., Stoklund Dittlau, K., and Van Den Bosch, L. (2020). Axonal transport defects and
608 neurodegeneration: Molecular mechanisms and therapeutic implications. Semin Cell Dev Biol 99,
609 133-150. 10.1016/j.semcdb.2019.07.010.

610 Hao, Y., Frey, E., Yoon, C., Wong, H., Nestorovski, D., Holzman, L.B., Giger, R.J., DiAntonio, A.,
611 and Collins, C. (2016). An evolutionarily conserved mechanism for cAMP elicited axonal
612 regeneration involves direct activation of the dual leucine zipper kinase DLK. Elife 5.
613 10.7554/eLife.14048.

614 Holland, S.M., Collura, K.M., Ketschek, A., Noma, K., Ferguson, T.A., Jin, Y., Gallo, G., and
615 Thomas, G.M. (2016). Palmitoylation controls DLK localization, interactions and activity to ensure
616 effective axonal injury signaling. Proc Natl Acad Sci U S A 113, 763-768.
617 10.1073/pnas.1514123113.

618 Huntwork-Rodriguez, S., Wang, B., Watkins, T., Ghosh, A.S., Pozniak, C.D., Bustos, D., Newton,
619 K., Kirkpatrick, D.S., and Lewcock, J.W. (2013). JNK-mediated phosphorylation of DLK
620 suppresses its ubiquitination to promote neuronal apoptosis. J Cell Biol 202, 747-763.
621 10.1083/jcb.201303066.

622 Karney-Grobe, S., Russo, A., Frey, E., Milbrandt, J., and DiAntonio, A. (2018). HSP90 is a
623 chaperone for DLK and is required for axon injury signaling. Proc Natl Acad Sci U S A 115, E9899-
624 E9908. 10.1073/pnas.1805351115.

625 Kim, J.H., Wang, X., Coolon, R., and Ye, B. (2013). Dscam expression levels determine
626 presynaptic arbor sizes in Drosophila sensory neurons. Neuron 78, 827-838.
627 10.1016/j.neuron.2013.05.020.

628 Klinedinst, S., Wang, X., Xiong, X., Haenfler, J.M., and Collins, C.A. (2013). Independent
629 pathways downstream of the Wnd/DLK MAPKKK regulate synaptic structure, axonal transport,
630 and injury signaling. J Neurosci 33, 12764-12778. 10.1523/JNEUROSCI.5160-12.2013.

631 Larhammar, M., Huntwork-Rodriguez, S., Jiang, Z., Solanoy, H., Sengupta Ghosh, A., Wang, B.,
632 Kaminker, J.S., Huang, K., Eastham-Anderson, J., Siu, M., et al. (2017a). Dual leucine zipper

633 kinase-dependent PERK activation contributes to neuronal degeneration following insult. Elife 6.
634 10.7554/eLife.20725.

635 Larhammar, M., Huntwork-Rodriguez, S., Rudhard, Y., Sengupta-Ghosh, A., and Lewcock, J.W.
636 (2017b). The Ste20 Family Kinases MAP4K4, MINK1, and TNIK Converge to Regulate Stress-
637 Induced JNK Signaling in Neurons. J Neurosci 37, 11074-11084. 10.1523/JNEUROSCI.0905-
638 17.2017.

639 Le Pichon, C.E., Meilandt, W.J., Dominguez, S., Solanoy, H., Lin, H., Ngu, H., Gogineni, A.,
640 Sengupta Ghosh, A., Jiang, Z., Lee, S.H., et al. (2017). Loss of dual leucine zipper kinase
641 signaling is protective in animal models of neurodegenerative disease. Sci Transl Med 9.
642 10.1126/scitranslmed.aag0394.

643 Lee, T., and Luo, L. (1999). Mosaic analysis with a repressible cell marker for studies of gene
644 function in neuronal morphogenesis. Neuron 22, 451-461. 10.1016/s0896-6273(00)80701-1.

645 Lee, W.C., Yoshihara, M., and Littleton, J.T. (2004). Cytoplasmic aggregates trap polyglutamine-
646 containing proteins and block axonal transport in a Drosophila model of Huntington's disease.
647 Proc Natl Acad Sci U S A 101, 3224-3229. 10.1073/pnas.0400243101.

648 Lewcock, J.W., Genoud, N., Lettieri, K., and Pfaff, S.L. (2007). The ubiquitin ligase Phr1 regulates
649 axon outgrowth through modulation of microtubule dynamics. Neuron 56, 604-620.
650 10.1016/j.neuron.2007.09.009.

651 Li, J., Zhang, Y.V., Asghari Adib, E., Stanchev, D.T., Xiong, X., Klinedinst, S., Soppina, P., Jahn,
652 T.R., Hume, R.I., Rasse, T.M., and Collins, C.A. (2017). Restraint of presynaptic protein levels by
653 Wnd/DLK signaling mediates synaptic defects associated with the kinesin-3 motor Unc-104. Elife
654 6. 10.7554/eLife.24271.

655 Li, Y., Ritchie, E.M., Steinke, C.L., Qi, C., Chen, L., Zheng, B., and Jin, Y. (2021). Activation of
656 MAP3K DLK and LZK in Purkinje cells causes rapid and slow degeneration depending on
657 signaling strength. Elife 10. 10.7554/eLife.63509.

658 Longo, P.A., Kavran, J.M., Kim, M.S., and Leahy, D.J. (2013). Transient mammalian cell
659 transfection with polyethylenimine (PEI). Methods Enzymol 529, 227-240. 10.1016/B978-0-12-
660 418687-3.00018-5.

661 Ma, X., Xu, W., Zhang, D., Yang, Y., Li, W., and Xue, L. (2015). Wallenda regulates JNK-mediated
662 cell death in Drosophila. Cell Death Dis 6, e1737. 10.1038/cddis.2015.111.

663 Martin, D.D.O., Kanuparthi, P.S., Holland, S.M., Sanders, S.S., Jeong, H.K., Einarson, M.B.,
664 Jacobson, M.A., and Thomas, G.M. (2019). Identification of Novel Inhibitors of DLK Palmitoylation
665 and Signaling by High Content Screening. Sci Rep 9, 3632. 10.1038/s41598-019-39968-8.

666 Miller, B.R., Press, C., Daniels, R.W., Sasaki, Y., Milbrandt, J., and DiAntonio, A. (2009). A dual
667 leucine kinase-dependent axon self-destruction program promotes Wallerian degeneration. Nat
668 Neurosci 12, 387-389. 10.1038/nn.2290.

669 Nakata, K., Abrams, B., Grill, B., Goncharov, A., Huang, X., Chisholm, A.D., and Jin, Y. (2005).
670 Regulation of a DLK-1 and p38 MAP kinase pathway by the ubiquitin ligase RPM-1 is required for
671 presynaptic development. Cell 120, 407-420. 10.1016/j.cell.2004.12.017.

672 Niu, J., Holland, S.M., Ketschek, A., Collura, K.M., Hesketh, N.L., Hayashi, T., Gallo, G., and
673 Thomas, G.M. (2022). Palmitoylation couples the kinases DLK and JNK3 to facilitate
674 prodegenerative axon-to-soma signaling. Sci Signal 15, eabh2674. 10.1126/scisignal.abh2674.

675 Niu, J., Sanders, S.S., Jeong, H.K., Holland, S.M., Sun, Y., Collura, K.M., Hernandez, L.M.,
676 Huang, H., Hayden, M.R., Smith, G.M., et al. (2020). Coupled Control of Distal Axon Integrity and
677 Somal Responses to Axonal Damage by the Palmitoyl Acyltransferase ZDHHC17. Cell Rep 33,
678 108365. 10.1016/j.celrep.2020.108365.

679 Patel, S., Cohen, F., Dean, B.J., De La Torre, K., Deshmukh, G., Estrada, A.A., Ghosh, A.S.,
680 Gibbons, P., Gustafson, A., Huestis, M.P., et al. (2015). Discovery of dual leucine zipper kinase
681 (DLK, MAP3K12) inhibitors with activity in neurodegeneration models. J Med Chem 58, 401-418.
682 10.1021/jm5013984.

683 Patel, S., Meilandt, W.J., Erickson, R.I., Chen, J., Deshmukh, G., Estrada, A.A., Fuji, R.N.,
684 Gibbons, P., Gustafson, A., Harris, S.F., et al. (2017). Selective Inhibitors of Dual Leucine Zipper
685 Kinase (DLK, MAP3K12) with Activity in a Model of Alzheimer's Disease. J Med Chem 60, 8083-
686 8102. 10.1021/acs.jmedchem.7b00843.

687 Pike, J.A., Styles, I.B., Rappoport, J.Z., and Heath, J.K. (2017). Quantifying receptor trafficking
688 and colocalization with confocal microscopy. Methods 115, 42-54. 10.1016/j.ymeth.2017.01.005.

689 Pozniak, C.D., Sengupta Ghosh, A., Gogineni, A., Hanson, J.E., Lee, S.H., Larson, J.L., Solanoy,
690 H., Bustos, D., Li, H., Ngu, H., et al. (2013). Dual leucine zipper kinase is required for
691 excitotoxicity-induced neuronal degeneration. J Exp Med 210, 2553-2567.
692 10.1084/jem.20122832.

693 Reddy, P.H., and Shirendeb, U.P. (2012). Mutant huntingtin, abnormal mitochondrial dynamics,
694 defective axonal transport of mitochondria, and selective synaptic degeneration in Huntington's
695 disease. Biochim Biophys Acta 1822, 101-110. 10.1016/j.bbadis.2011.10.016.

696 Saha, A.R., Hill, J., Utton, M.A., Asuni, A.A., Ackerley, S., Grierson, A.J., Miller, C.C., Davies,
697 A.M., Buchman, V.L., Anderton, B.H., and Hanger, D.P. (2004). Parkinson's disease alpha-
698 synuclein mutations exhibit defective axonal transport in cultured neurons. J Cell Sci 117, 1017-
699 1024. 10.1242/jcs.00967.

700 Seong, K.H., Matsuo, T., Fuyama, Y., and Aigaki, T. (2001). Neural-specific overexpression of
701 drosophila plenty of SH3s (DPOSH) extends the longevity of adult flies. Biogerontology 2, 271-
702 281. 10.1023/a:1013249326285.

703 Shin, J.E., Cho, Y., Beirowski, B., Milbrandt, J., Cavalli, V., and DiAntonio, A. (2012). Dual leucine
704 zipper kinase is required for retrograde injury signaling and axonal regeneration. Neuron 74,
705 1015-1022. 10.1016/j.neuron.2012.04.028.

706 Singh, M., Ye, B., and Kim, J.H. (2022). Dual Leucine Zipper Kinase Regulates Dscam Expression
707 through a Noncanonical Function of the Cytoplasmic Poly(A)-Binding Protein. J Neurosci 42,
708 6007-6019. 10.1523/JNEUROSCI.0543-21.2022.

709 Smith, G.A., Rocha, E.M., McLean, J.R., Hayes, M.A., Izen, S.C., Isacson, O., and Hallett, P.J.
710 (2014). Progressive axonal transport and synaptic protein changes correlate with behavioral and
711 neuropathological abnormalities in the heterozygous Q175 KI mouse model of Huntington's
712 disease. Hum Mol Genet 23, 4510-4527. 10.1093/hmg/ddu166.

713 Sterne, G.R., Kim, J.H., and Ye, B. (2015). Dysregulated Dscam levels act through Abelson
714 tyrosine kinase to enlarge presynaptic arbors. Elife 4. 10.7554/eLife.05196.

715 Stowers, R.S., and Isacoff, E.Y. (2007). Drosophila huntingtin-interacting protein 14 is a
716 presynaptic protein required for photoreceptor synaptic transmission and expression of the
717 palmitoylated proteins synaptosome-associated protein 25 and cysteine string protein. J Neurosci
718 27, 12874-12883. 10.1523/JNEUROSCI.2464-07.2007.

719 Tortosa, E., and Hoogenraad, C.C. (2018). Polarized trafficking: the palmitoylation cycle
720 distributes cytoplasmic proteins to distinct neuronal compartments. Curr Opin Cell Biol 50, 64-71.
721 10.1016/j.ceb.2018.02.004.

722 Tortosa, E., Sengupta Ghosh, A., Li, Q., Wong, W.R., Hinkle, T., Sandoval, W., Rose, C.M., and
723 Hoogenraad, C.C. (2022). Stress-induced vesicular assemblies of dual leucine zipper kinase are
724 signaling hubs involved in kinase activation and neurodegeneration. EMBO J 41, e110155.
725 10.15252/embj.2021110155.

726 Valakh, V., Frey, E., Babetto, E., Walker, L.J., and DiAntonio, A. (2015). Cytoskeletal disruption
727 activates the DLK/JNK pathway, which promotes axonal regeneration and mimics a
728 preconditioning injury. Neurobiol Dis 77, 13-25. 10.1016/j.nbd.2015.02.014.

729 Valakh, V., Walker, L.J., Skeath, J.B., and DiAntonio, A. (2013). Loss of the spectraplakin short
730 stop activates the DLK injury response pathway in Drosophila. J Neurosci 33, 17863-17873.
731 10.1523/JNEUROSCI.2196-13.2013.

732 Venken, K.J., Schulze, K.L., Haelterman, N.A., Pan, H., He, Y., Evans-Holm, M., Carlson, J.W.,
733 Levis, R.W., Spradling, A.C., Hoskins, R.A., and Bellen, H.J. (2011). MiMIC: a highly versatile
734 transposon insertion resource for engineering Drosophila melanogaster genes. Nat Methods 8,
735 737-743. 10.1038/nmeth.1662.

736 Wang, X., Kim, J.H., Bazzi, M., Robinson, S., Collins, C.A., and Ye, B. (2013). Bimodal control of
737 dendritic and axonal growth by the dual leucine zipper kinase pathway. PLoS Biol 11, e1001572.
738 10.1371/journal.pbio.1001572.

739 Wang, Z.X., Tan, L., and Yu, J.T. (2015). Axonal transport defects in Alzheimer's disease. Mol
740 Neurobiol 51, 1309-1321. 10.1007/s12035-014-8810-x.

741 Watkins, T.A., Wang, B., Huntwork-Rodriguez, S., Yang, J., Jiang, Z., Eastham-Anderson, J.,
742 Modrusan, Z., Kaminker, J.S., Tessier-Lavigne, M., and Lewcock, J.W. (2013). DLK initiates a
743 transcriptional program that couples apoptotic and regenerative responses to axonal injury. Proc
744 Natl Acad Sci U S A 110, 4039-4044. 10.1073/pnas.1211074110.

745 Welsbie, D.S., Yang, Z., Ge, Y., Mitchell, K.L., Zhou, X., Martin, S.E., Berlinicke, C.A., Hackler,
746 L., Fuller, J., Fu, J., et al. (2013). Functional genomic screening identifies dual leucine zipper
747 kinase as a key mediator of retinal ganglion cell death. Proc Natl Acad Sci U S A 110, 4045-4050.
748 10.1073/pnas.1211284110.

749 Welsbie, D.S., Mitchell, K.L., Jaskula-Ranga, V., Sluch, V.M., Yang, Z., Kim, J., Buehler, E., Patel,
750 A., Martin, S.E., Zhang, P.W., et al. (2017). Enhanced Functional Genomic Screening Identifies
751 Novel Mediators of Dual Leucine Zipper Kinase-Dependent Injury Signaling in Neurons. Neuron
752 94, 1142-1154.e1146. 10.1016/j.neuron.2017.06.008.

753 Wu, C., Wairkar, Y.P., Collins, C.A., and DiAntonio, A. (2005). Highwire function at the Drosophila
754 neuromuscular junction: spatial, structural, and temporal requirements. J Neurosci 25, 9557-
755 9566. 10.1523/JNEUROSCI.2532-05.2005.

756 Xiong, X., and Collins, C.A. (2012). A conditioning lesion protects axons from degeneration via
757 the Wallenda/DLK MAP kinase signaling cascade. J Neurosci 32, 610-615.
758 10.1523/JNEUROSCI.3586-11.2012.

759 Xiong, X., Hao, Y., Sun, K., Li, J., Li, X., Mishra, B., Soppina, P., Wu, C., Hume, R.I., and Collins,
760 C.A. (2012). The Highwire ubiquitin ligase promotes axonal degeneration by tuning levels of
761 Nmnat protein. PLoS Biol 10, e1001440. 10.1371/journal.pbio.1001440.

762 Xiong, X., Wang, X., Ewanek, R., Bhat, P., Diantonio, A., and Collins, C.A. (2010). Protein
763 turnover of the Wallenda/DLK kinase regulates a retrograde response to axonal injury. J Cell Biol
764 191, 211-223. 10.1083/jcb.201006039.

765 Yan, D., Wu, Z., Chisholm, A.D., and Jin, Y. (2009). The DLK-1 kinase promotes mRNA stability
766 and local translation in C. elegans synapses and axon regeneration. Cell 138, 1005-1018.
767 10.1016/j.cell.2009.06.023.

768 Ye, B., Zhang, Y., Song, W., Younger, S.H., Jan, L.Y., and Jan, Y.N. (2007). Growing dendrites
769 and axons differ in their reliance on the secretory pathway. Cell 130, 717-729.
770 10.1016/j.cell.2007.06.032.

771 Zhou, W., Chang, J., Wang, X., Savelieff, M.G., Zhao, Y., Ke, S., and Ye, B. (2014). GM130 is
772 required for compartmental organization of dendritic golgi outposts. Curr Biol 24, 1227-1233.
773 10.1016/j.cub.2014.04.008.

Figure 1

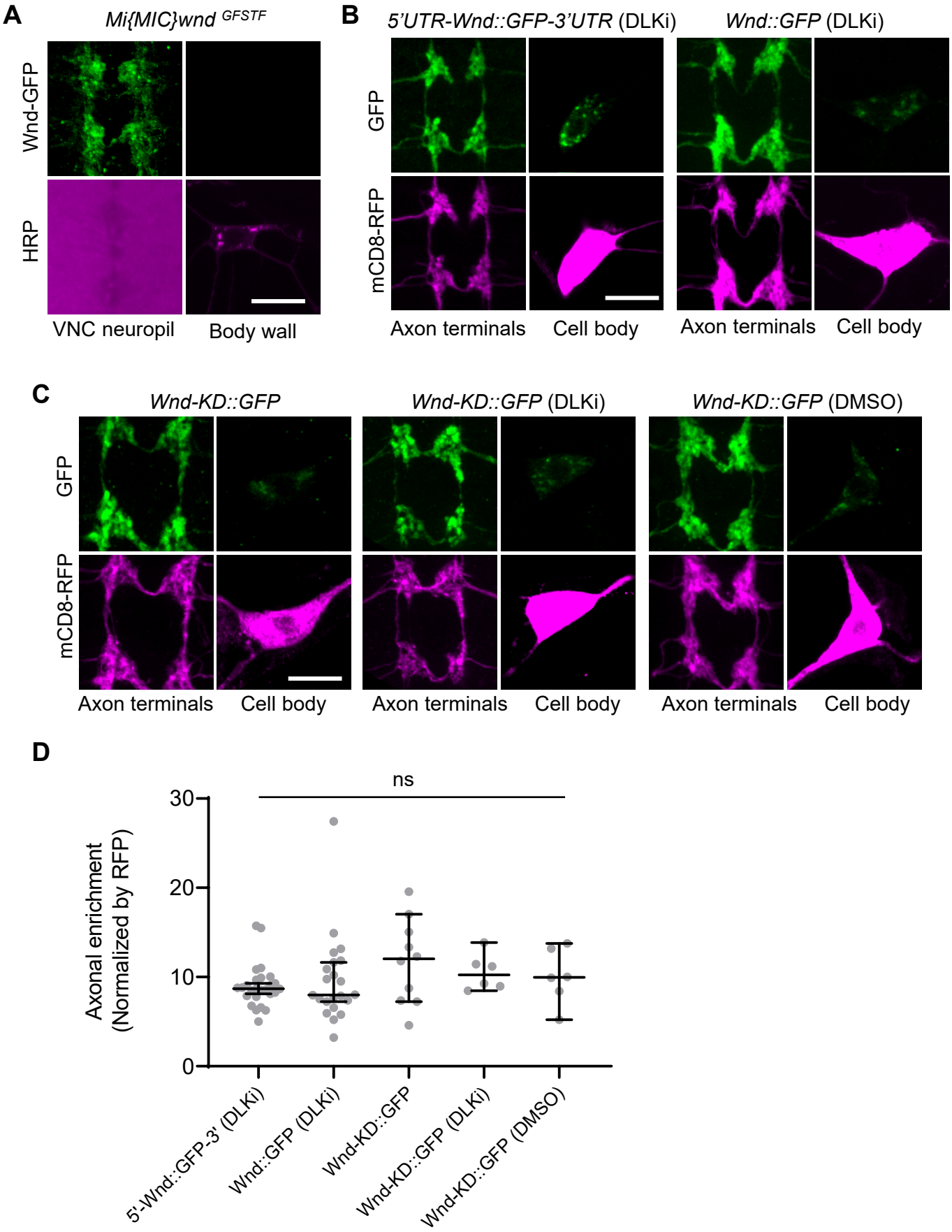
A
Mi{MIC}wnd GFSTF
Wnd-GFP
HRP
VNC neuropil
Body wall
B
5'UTR-Wnd::GFP-3'UTR (DLKi)
Wnd::GFP (DLKi)
GFP
mCD8-RFP
Axon terminals
Cell body
Axon terminals
Cell body
C
Wnd-KD::GFP
Wnd-KD::GFP (DLKi)
Wnd-KD::GFP (DMSO)
GFP
mCD8-RFP
Axon terminals
Cell body
Axon terminals
Cell body
Axon terminals
Cell body
D
ns
Axonal enrichment
(Normalized by RFP)
30
20
10
0
5'-Wnd::GFP-3' (DLKi)
Wnd::GFP (DLKi)
Wnd-KD::GFP
Wnd-KD::GFP (DLKi)
Wnd-KD::GFP (DMSO)

Figure 2

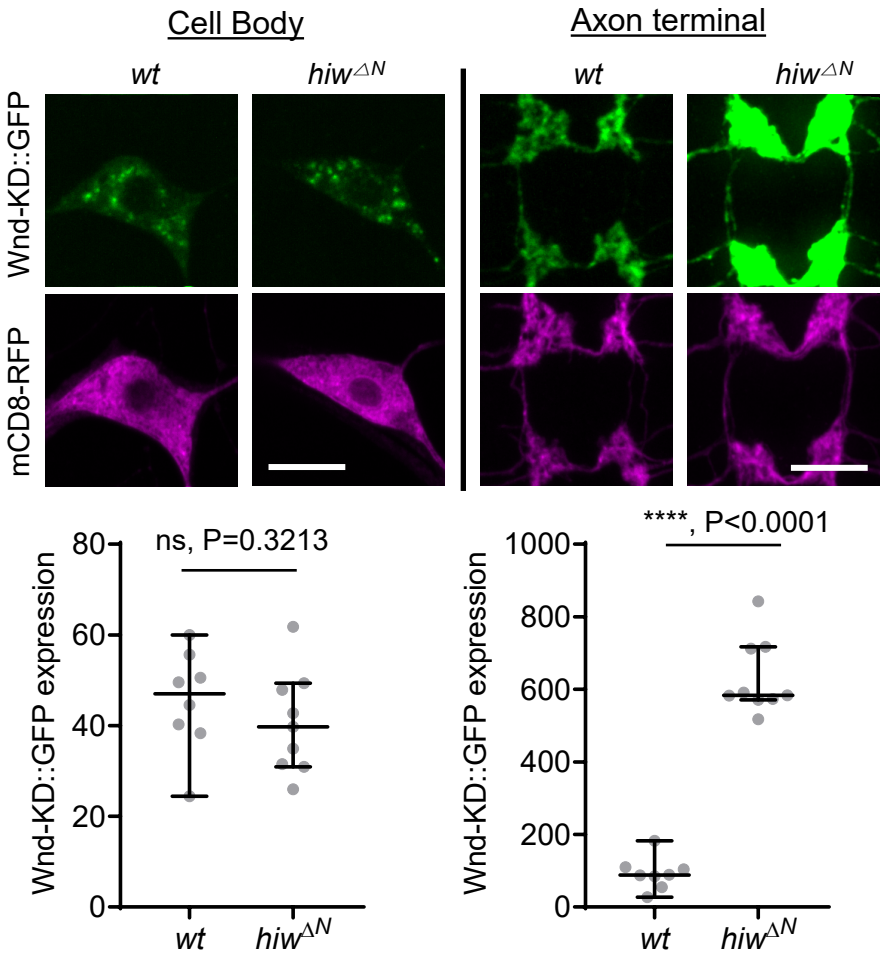
Cell Body
Axon terminal
wt
hiwΔN
wt
hiwΔN
Wnd-KD::GFP
mCD8-RFP
ns, P=0.3213
Wnd-KD::GFP expression
80
60
40
20
0
wt
hiwΔN
****, P<0.0001
Wnd-KD::GFP expression
1000
800
600
400
200
0
wt
hiwΔN

Figure 3

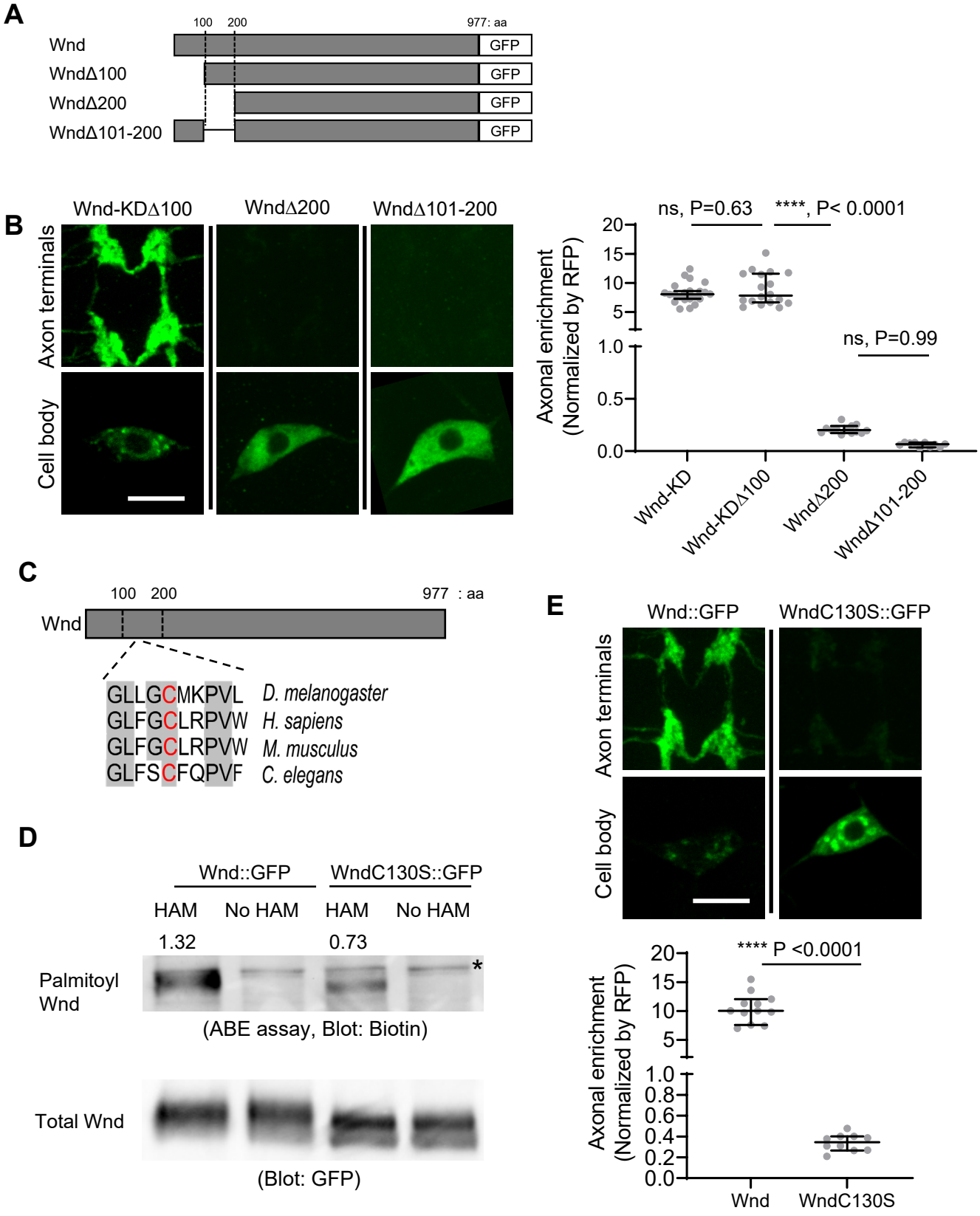
A
100
200
977: aa
Wnd
WndΔ100
WndΔ200
WndΔ101-200
GFP
B
Wnd-KDΔ100
WndΔ200
WndΔ101-200
Axon terminals
Cell body
ns, P=0.63
****, P< 0.0001
ns, P=0.99
Axonal enrichment
(Normalized by RFP)
Wnd-KD
Wnd-KDΔ100
WndΔ200
WndΔ101-200
C
100
200
977 : aa
Wnd
GLLGCMKPVL D. melanogaster
GLFGCLRPVW H. sapiens
GLFGCLRPVW M. musculus
GLFSCFQPVF C. elegans
D
Wnd::GFP
WndC130S::GFP
HAM
No HAM
HAM
No HAM
1.32
0.73
Palmitoyl Wnd
(ABE assay, Blot: Biotin)
Total Wnd
(Blot: GFP)
E
Wnd::GFP
WndC130S::GFP
Axon terminals
Cell body
**** P <0.0001
Axonal enrichment
(Normalized by RFP)
Wnd
WndC130S

Figure 4

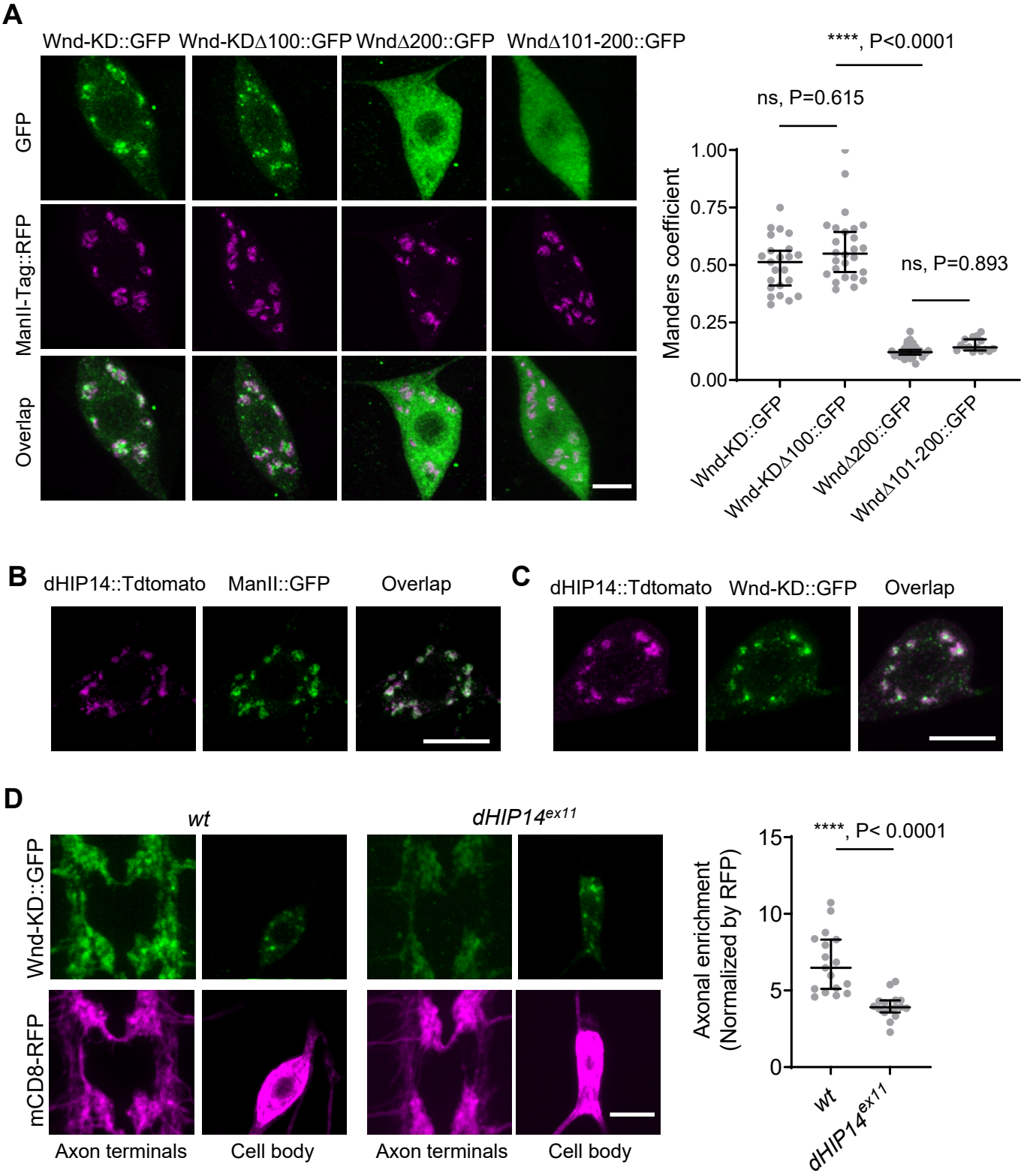
A
Wnd-KD::GFP
Wnd-KDΔ100::GFP
WndΔ200::GFP
WndΔ101-200::GFP
GFP
ManII-Tag::RFP
Overlap
****, P<0.0001
ns, P=0.615
ns, P=0.893
Manders coefficient
1.00
0.75
0.50
0.25
0.00
Wnd-KD::GFP
Wnd-KDΔ100::GFP
WndΔ200::GFP
WndΔ101-200::GFP
B
dHIP14::Tdtomato
ManII::GFP
Overlap
C
dHIP14::Tdtomato
Wnd-KD::GFP
Overlap
D
wt
dHIP14ex11
Wnd-KD::GFP
mCD8-RFP
Axon terminals
Cell body
Axon terminals
Cell body
****, P< 0.0001
Axonal enrichment
(Normalized by RFP)
15
10
5
0
wt
dHIP14ex11

Figure 5

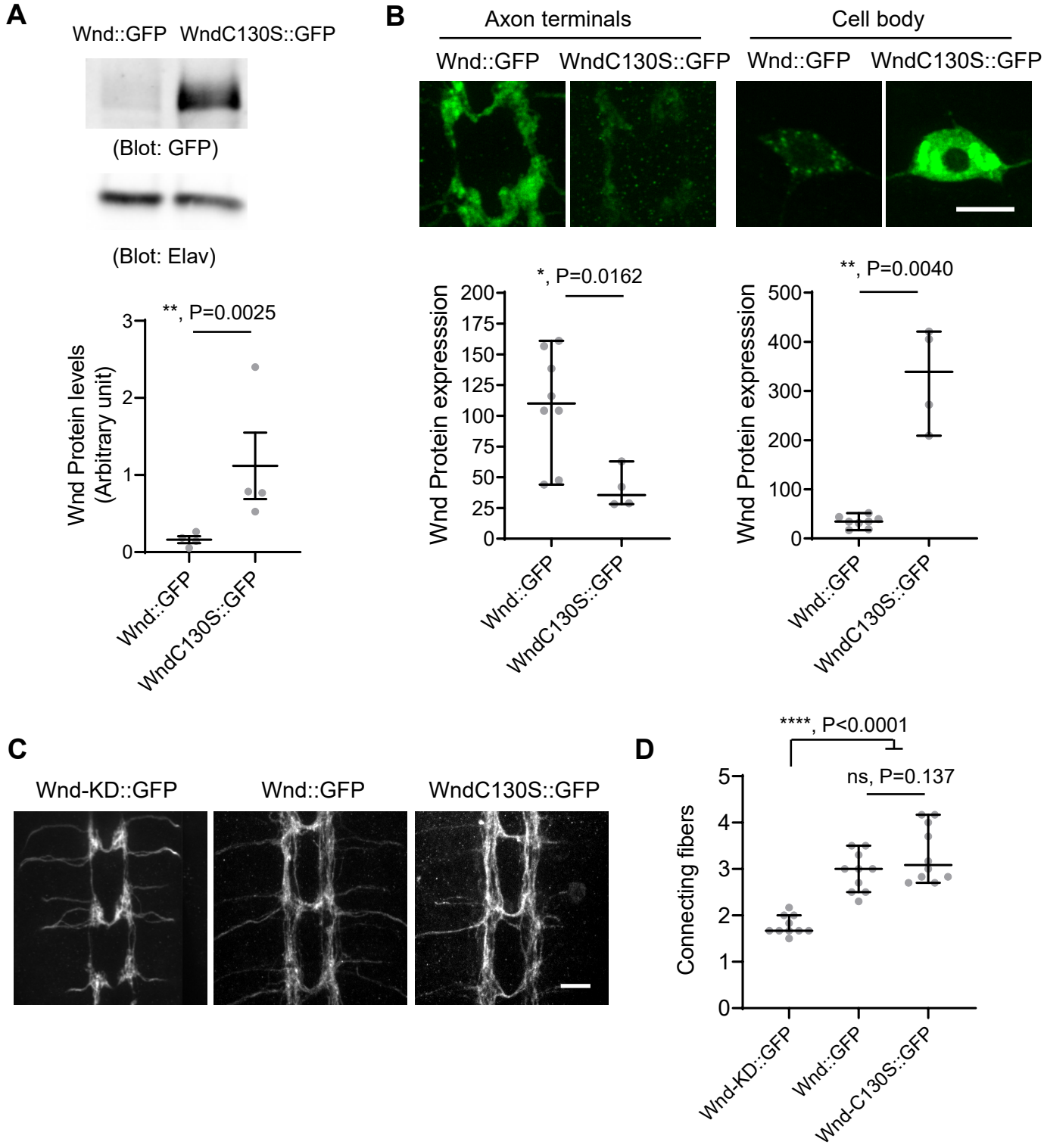
A
Wnd::GFP
WndC130S::GFP
(Blot: GFP)
(Blot: Elav)
**, P=0.0025
Wnd Protein levels (Arbitrary unit)
Wnd::GFP
WndC130S::GFP
B
Axon terminals
Cell body
Wnd::GFP
WndC130S::GFP
*, P=0.0162
**, P=0.0040
Wnd Protein expresssion
C
Wnd-KD::GFP
Wnd::GFP
WndC130S::GFP
D
****, P<0.0001
ns, P=0.137
Connecting fibers
Wnd-KD::GFP
Wnd::GFP
Wnd-C130S::GFP

Figure 6

A

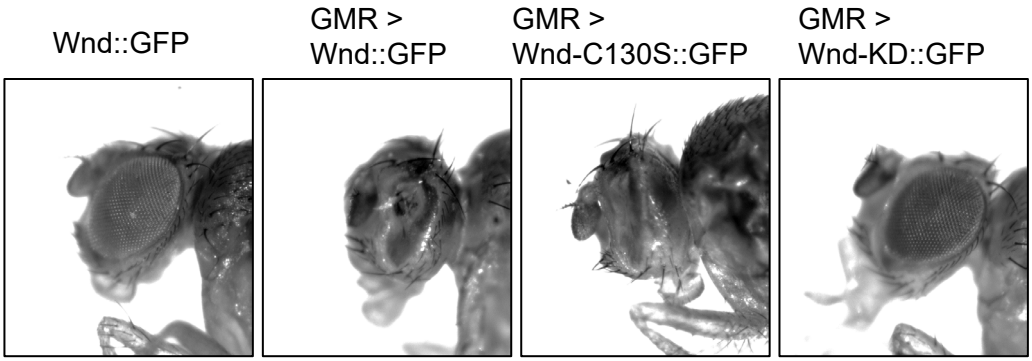
Wnd::GFP
GMR > Wnd::GFP
GMR > Wnd-C130S::GFP
GMR > Wnd-KD::GFP

B

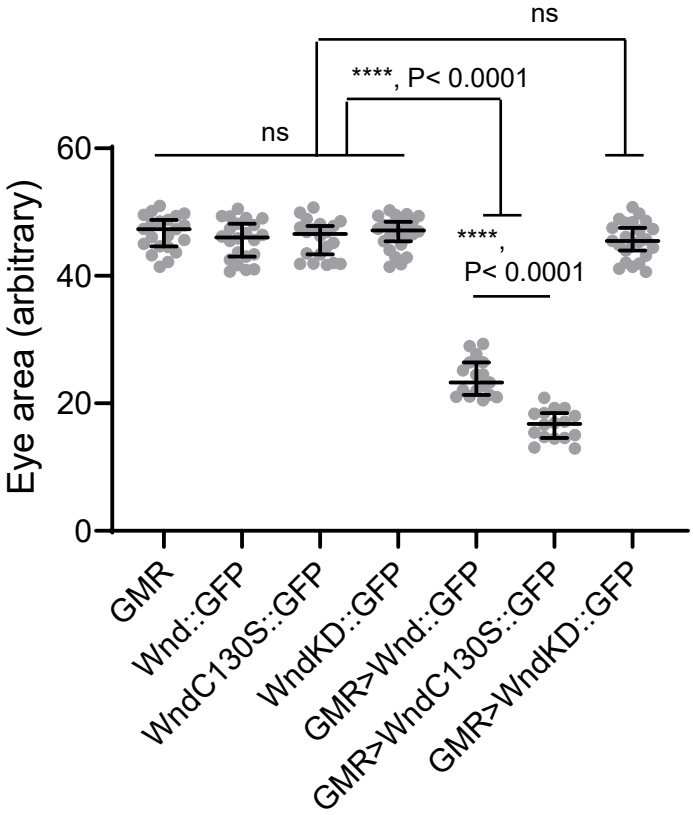
ns
****, P< 0.0001
ns
****, P< 0.0001
Eye area (arbitrary)
60
40
20
0
GMR
Wnd::GFP
WndC130S::GFP
WndKD::GFP
GMR>Wnd::GFP
GMR>WndC130S::GFP
GMR>WndKD::GFP